Ali, Abdelfatah; Mahmoud, Karar; Lehtonen, Matti

Optimal planning of inverter-based renewable energy sources towards autonomous microgrids accommodating electric vehicle charging stations

Published in:
IET GENERATION TRANSMISSION AND DISTRIBUTION

DOI:
10.1049/gtd2.12268

Published: 01/01/2022

Document Version
Publisher's PDF, also known as Version of record

Received: 29 April 2021 | Revised: 17 July 2021 | Accepted: 28 July 2021

IET Generation, Transmission & Distribution

DOI: 10.1049/gtd2.12268

The Institution of Engineering and Technology WILEY

ORIGINAL RESEARCH PAPER

Optimal planning of inverter-based renewable energy sources towards autonomous microgrids accommodating electric vehicle charging stations

Abdelfatah Ali[1] | **Karar Mahmoud**[2,3] | **Matti Lehtonen**[2]

[1] Department of Electrical Engineering, South Valley University, Qena 83523, Egypt

[2] Department of Electrical Engineering and Automation, Aalto University, Espoo FI-00076, Finland

[3] Department of Electrical Engineering, Aswan University, Aswan 81542, Egypt

Correspondence
Karar Mahmoud, Department of Electrical Engineering and Automation, Aalto University, FI-00076 Espoo, Finland.
Email: karar.mostafa@aalto.fi

Abstract

Renewable energy sources have recently been integrated into microgrids that are in turn connected to electric vehicle (EV) charging stations. In this regard, the optimal planning of microgrids is challenging with such uncertain generation and stochastic charging/discharging EV models. To achieve such ambitious goals, the best sites and sizes of photovoltaic and wind energy units in microgrids with EV are accurately determined in this work using an optimization technique. This proposed technique considers 1) generation profile uncertainty in photovoltaic and wind energy units as well as the total load demand, 2) photovoltaic and wind generation units' DSTATCOM operation capability, and 3) various branch and node constraints in the microgrid. Most importantly, the possible EV requirements are also taken into account, including initial and predetermined state of charge (SOC) arrangements, arrival and departure hours, and diverse regulated and unregulated charging strategies. A bi-level metaheuristic-based solution is established to address this complex planning model. The outer level and inner-level functions optimize renewable energy sources and EV decision variables. Sub-objectives to be optimized voltage deviations as well as grid power. The results demonstrate the effectiveness of the introduced method for planning renewable energy sources and managing EV to effectively achieve autonomous microgrids.

1 | INTRODUCTION

Renewable energy sources (RESs) are being more widely used around the world. Global policies to minimize greenhouse gas emissions drive this trend, but innovations in future electrical power generation technologies are anticipated [1–3]. Due to their elasticity and cost-effectiveness, photovoltaic (PV) and wind turbine (WT) are the most prominent RES variants. Remarkably, RESs have the potential to have a positive impact on distribution system efficiency. Such PV and WT systems, in particular, could improve supply efficiency, solve voltage problems, reduce power losses, improve power quality, and reduce the loading on traditional controlling units, thanks to their smart functions [4, 5]. However, the PV and WT units' extremely intermittent generation could cause a slew of functional and operational issues, limiting their authorized accommodating capacities in the grid [6–8]. In line with the rising popularity of PV and WT, interest in electric vehicles (EVs) has been growing rapidly around the world [9, 10].

There is a growing interest in the recent literature for determining the sites and sizes of various RESs in distribution systems to enhance various grid performance indices. The authors of [11] have proposed a two-stage data-driven robust optimization model (for placement RESs, considering both load and generation uncertainties to minimize the total installation and operational costs. In [12], a probabilistic model has been introduced to allocate different RESs in distribution systems to maximize energy loss mitigation while still meeting system limits. A novel fast yet accurate approach for optimally sizing PV in distribution systems based on machine learning has been proposed in [13] to minimize energy losses. Different analytically based approaches are proposed in [14, 15] that can deliver

fast results in terms of the optimal sizes and sites of multiple PV and WT systems by considering expected load/generation conditions. In [16], a multi-objective method for efficiently planning PV and WT systems in distribution networks has been proposed, taking into account their probabilistic frameworks while minimizing emissions and total costs. Wide varieties have been used for RES planning in distribution systems, particularly for multi-objective structures, resulting from recent revolutions in implementing and sustaining effective meta-heuristic optimization problem solvers. Crow search algorithm autodrive particle swarm optimization method [17], gravitational search algorithm [18, 19], tabu search optimization solver [20], genetic-based optimization method [21], artificial ecosystem-based optimization method [22], equilibrium optimizer [23], simulated annealing optimization method [24], and ant colony optimization method [25] are some examples of optimization solvers. The authors of [26] have proposed an adaptive robust co-optimization method for capacity allocation and bidding approach of a prosumer interconnected with PV, WT, and a battery energy storage system. The importance of energy storage systems and EVs in increasing RES hosting flexibility has been investigated in [27]. In [28], a new planning model for wind-based DGs and fast-charging stations has been proposed considering residential loads and renewable power generation.

In [29], the long-term capacity expansion planning model is investigated in microgrids interconnected to EVs and various RES types. The authors of [30] have examined the generation planning problem in island microgrids with RES to reduce environmental impact. In [31], a technique for optimum design of a DC microgrid for electric vehicle supply infrastructure has been proposed with considering various converter types and topologies. In [32], a two-level problem is presented for isolated microgrids with EVs. The authors of [33] have proposed a method for planning microgrids with EV charging demand to determine the most economical configuration for maximizing RES utilization. In [34], a comprehensive framework for optimally planning and operating EV batteries has been proposed for microgrids. In [35], a study for the impacts of EV integration approaches has been performed on utility grids' operation. Accordingly, most of the suggested work is based on assumptions to simplify the RES with the EVs planning model. Some of these approaches assume a single RES allocation or use deterministic RES and load models, but they do not take EVs into account. Even techniques that take into account the intermittent and unpredictable nature of RES and loads ignore the presence of EVs. The present techniques in the RES allocation problem do not take into account the various control systems of EVs units, their stochastic character, or their detailed model. As a result, further research and development are still needed to solve this RES allocation model in microgrids.

As demonstrated above, with the uncertain generation of photovoltaic and wind energy systems and stochastic charging/discharging EV models, microgrids' economic and optimal operation is problematic. In this work, the optimal locations and sizes of photovoltaic and wind energy units in microgrids with EV charging stations are precisely calculated using an optimization technique to achieve autonomous microgrids. The novelty of the suggested approach includes taking into account RES and load uncertainty, as well as the stochastic character of EVs. Besides, the optimization model considers EV operation restrictions such as various charging control schemes of EVs, including controlled and uncontrolled charging strategies. This technique takes into account generation profile intermittency in photovoltaic and wind energy systems, as well as overall load demand, DSTATCOM operating ability of inverter-based photovoltaic and wind generation stations, and various branch and node constraints in the microgrid. EV conditions, such as initial and predetermined state of charge (SOC) arrangements, arrival and departure hours, and various controlled and uncontrolled charging strategies, are also considered. To solve this multipart planning model accurately, we established a bi-level metaheuristic-based optimization approach. Renewable energy sources and EV decision variables are optimized using the outer level (main problem) and inner level (sub-problem) functions, respectively. Total voltage deviations, as well as grid energy, are treated as sub-objectives to be optimized. A series of tests and case studies are used to assess the viability of the proposed solution. The conclusions show that the proposed approach for planning renewable energy sources and controlling EVs effectively achieves autonomous microgrids with photovoltaic, wind, and EV charging stations.

2 | PROPOSED RES PLANNING MODEL

The planning model for planning PV and WT units in microgrids integrated with EV charging stations is described in this section. Owing to the incorporation of PV and WT in the microgrid, the tie-line control between the utility network and the microgrid may have high volatility, which may trigger various technical issues such as voltage fluctuations and severe voltage deviations. Besides, reducing tie-line control reduces the microgrid's autonomy. As a result, the tie-line power and energy deficits are used here as sub-objectives in the planning problem to be reduced. Below, we describe in detail the panning model of PV and WT units considering the various constraints.

2.1 | Objective function

$$\text{Minimize}\{F1, F2\} \tag{1}$$

in which $F1$ and $F2$ represent, respectively, the total voltage deviations in the distribution system and the tie-line power, which are formulated as:

2.1.1 | Voltage deviations

The total voltage deviations in the distribution system can be formulated as follows:

$$F1 = \sum_{t=1}^{n_t} \sum_{s=1}^{n_s} VD_s^t \times PM \tag{2}$$

in which

$$VD_s^t = \sum_{i=1}^{N_B} \left(\frac{V_i - V_n}{V_n} \right)^2 \tag{3}$$

where VD_s^t represents the total voltage deviations in the microgrid, whose number of buses is N_B at time instant t during state s. Note that n_t and n_s represents, respectively, the number of time instants as well as the states' number. V_i and V_n are, respectively, the voltage at node i and the normal voltage (1 pu). It is worth noting that we have considered a complete probability model (denoted by *PM*) for wind speed, solar irradiance, and total load, where the detailed formulation is given in previous work [18], [19].

2.1.2 | Tie-line power

$$F2 = \sum_{t=1}^{n_t} \sum_{s=1}^{n_s} P_{TL,s}^t \times PM \tag{4}$$

in which $P_{TL,s}^t$ represents the amount of tie-line power fed by the main grid to the microgrid.

2.1.3 | Constraints

$$\begin{aligned} &N_{WTi} P_{WT,i,s}^t + P_{PV,i,s}^t + P_{Diesel,i,s}^t - P_{D,i,s}^t \pm P_{C,i,s}^t \\ &- V_{i,s}^t \sum_{j=1}^{n_b} \begin{matrix} V_{j,s}^t [G_{ij} \cos \delta_{ij,s}^t \\ + B_{ij} \sin \delta_{ij,s}^t] \end{matrix} = 0 \end{aligned} \tag{5}$$

$$\begin{aligned} &N_{WTi} Q_{I,WT,i,s}^t + Q_{I,PV,i,s}^t + Q_{Diesel,i,s}^t - Q_{D,i,s}^t \\ &- V_{i,s}^t \sum_{j=1}^{n_b} V_{j,s}^t \begin{bmatrix} G_{ij} \sin \delta_{ij,s}^t \\ + B_{ij} \cos \delta_{ij,s}^t \end{bmatrix} = 0, \\ &\forall i \notin \phi_b, s, t \end{aligned} \tag{6}$$

$$V^{min} \le V_{i,s}^t \le V^{max}, \ \forall i \in \phi_b, s, t \tag{7}$$

$$P_{C,i,s}^{min,t} \le P_{C,i,s}^t \le P_{C,i,s}^{max,t}, \ \forall i \in \phi_b, s, t \tag{8}$$

$$P_{Diesel,i,s}^{min,t} \le P_{Diesel,i,s}^t \le P_{Diesel,i,s}^{max,t}, \ \forall i \in \phi_b, s, t \tag{9}$$

$$N_{WTi}^{min} \le N_{WTi} \le N_{WTi}^{max}, \ \forall i \in \phi_b \tag{10}$$

$$C_{PV,i}^{min} \le C_{PV,i} \le C_{PV,i}^{max}, \ \forall i \in \phi_b \tag{11}$$

$$C_{WT,i}^{min} \le C_{WT,i} \le C_{WT,i}^{max}, \ \forall i \in \phi_b \tag{12}$$

$$\sum_{i=1}^{N_{PV}} P_{PV,i} \le R_{PV}^{max} \tag{13}$$

$$\sum_{i=1}^{N_{WT}} P_{WT,i} \le R_{WT}^{max} \tag{14}$$

$$Q_{Diesel,i,s}^{min,t} \le Q_{Diesel,i,s}^t \le Q_{Diesel,i,s}^{max,t}, \ \forall i \in \phi_b, s, t \tag{15}$$

$$Q_{I,PV,i,s}^{min,t} \le Q_{I,PV,i,s}^t \le Q_{I,PV,i,s}^{max,t}, \ \forall i \in \phi_b, s, t \tag{16}$$

$$Q_{I,WT,i,s}^{min,t} \le Q_{I,WT,i,s}^t \le Q_{I,WT,i,s}^{max,t}, \ \forall i \in \phi_b, s, t \tag{17}$$

$$\begin{cases} Q_{I,PV,i,s}^{max,t} = \sqrt{S_{I,PV,i}^2 - \left(P_{PV,i,s}^t\right)^2} \\ Q_{I,PV,i,s}^{min,t} = -\sqrt{S_{I,PV,i}^2 - \left(P_{PV,i,s}^t\right)^2} \end{cases} \tag{18}$$

$$\begin{cases} Q_{I,WT,i,s}^{max,t} = \sqrt{S_{I,WT,i}^2 - \left(P_{WT,i,s}^t\right)^2} \\ Q_{I,WT,i,s}^{min,t} = -\sqrt{S_{I,WT,i}^2 - \left(P_{WT,i,s}^t\right)^2} \end{cases} \tag{19}$$

$$SOC_{n,d,s} \ge SOC_{n,min,s} \tag{20}$$

$$I_{ij,s}^t \le I_{ij}^{max}, \ \forall ij, s, t \tag{21}$$

Equations (1)–(4) denote the objective function, while Equations (5), (6) and (7)–(21) represent the equality constraints and inequality constraints, respectively, of *PV*, *WT*, *EV*, diesel generators, and the distribution system. Equations (7)–(12) ensure that the voltage level, charging station power, diesel generator power, number of WT units, *PV* unit capacity, and *WT* unit capacity across all the microgrid nodes are kept within desired limits, respectively. On the other hand, the desired limits of the reactive power injected/absorbed by the diesel generator and interfacing inverters of RES are given in Equations (15)–(17), while the minimum limit of the SOC of each EV at departure time is given in Equation (20). The line thermal capacities are described in Equation (21). Note that we have used an index subscript i in Equations (5)–(20) to indicate the RES location while the sizing of RES is mentioned in Equations (11) and (12). G_{ij} and B_{ij} stand for the values of the conductance and susceptance of the branch ij in the microgrid with n_b nodes. $V_{i,s}^t$ and $\delta_{ij,s}^t$ stand for, respectively, the voltage magnitude and angle at node i; $N_{WT,i}$ represents the numbers of *WT* units integrated at bus i. The output generation of *PV*, *WT*, and diesel generator at bus i are represented by $P_{PV,i,s}^t$, $P_{WT,i,s}^t$, and $P_{Diesel,i,s}^t$, respectively, while the total demand of reactive power is denoted by $Q_{D,i}^t$. $P_{D,i}^t$ and $P_{C,j,s}^t$ symbolize the total active load demand and charging station of *EV*, respectively. $C_{PV,i}$ and $C_{WT,i}$ stand for the sizes of *PV* and *WT* systems, respectively, while the highest allowed total *PV*, and *WT* capacities are symphonized by R_{PV}^{max} and R_{WT}^{max}, respectively. Regarding the interacting inverter of *PV*, its rated capacity is denoted by $S_{I,PV,i}$ while the corresponding reactive power contribution is $Q_{I,PV,i,s}^t$ at

ith node. In turn, regarding the interacting inverter of WT, its rated capacity is denoted by $S_{I,WT,i}$ while its corresponding reactive power contribution is $Q^t_{I,WT,i,s}$ at ith node. Further, the reactive power of the diesel generator is represented by $Q^t_{Diesel,i,s}$.Vector ϕ_b involves system buses. With respect to the EV model, $SOC_{n,d,s}$ characterizes the amount of state of charge (SOC) of nth EV battery at parting time. In turn, $SOC_{n,min,s}$ characterizes the least SOC selected by the EV operator. The probability model (PM) includes an integrated set of the solar irradiance probability ($prob^t_R(G_x)$), wind speed probability ($prob^t_w(G_y)$), and load demand probability ($prob^t_l(G_z)$), which is represented by:

$$PM^t(\lambda_s) = prob^t_R(G_x) \times prob^t_w(G_y) \times prob^t_l(G_z) \quad (22)$$

Then, the PM is constructed for all possible solar irradiance, wind speed, and load combinations. Therefore, the complete PM (ψ) is represented by:

$$\psi = [\{\lambda_s, PM(\lambda_s)\} : s = 1 : n_S] \quad (23)$$

in which $PM(\lambda_s)$ involves the components of the PM based on the matrix λ. It is worth mentioning that Beta pdf, Weibull pdf, and normal pdf are employed to model the solar irradiance, the wind speed, and the load demand, respectively. The detailed modelling of the EV battery and the stochastic model can be founded in [36–38].

3 | MULTI-OBJECTIVE GREY WOLF OPTIMIZER (MOGWO)

3.1 | Optimization algorithm

The grey wolf optimization (GWO) algorithm is a new meta-heuristic algorithm and it was developed in [39]. The main inspiration of this algorithm is the social leadership and hunting technique of grey wolves. The GWO is firstly developed to solve a single-objective optimization problem. The main operators needed for the reproduction process include social hierarchy, encircling prey, hunting and attacking prey, and searching for prey.

During designing GWO, to model the social hierarchy of wolves, the best, second best, and third best solutions are denoted by alpha (α), beta (β), and delta (δ) wolves, respectively. On the other hand, the candidate solutions' remainders are represented by omega (ω) wolves. The hunting in this algorithm is driven by α, β, and δ wolves while the rest wolves (ω) follow them in the search for the global optimal. To simulate the behaviour of encircling for the wolves during the hunt, the following formulas are developed:

$$\vec{D} = \left|\vec{C}.\vec{X}_p(t) - \vec{X}(t)\right| \quad (24)$$

$$\vec{X}(t+1) = \vec{X}_p(t) - \vec{A}.\vec{D} \quad (25)$$

where t represents the current iteration; $\vec{A}$ and $\vec{C}$ represent the coefficient vectors; $\vec{X}_p$ represents the position vector of the victim; $\vec{X}$ is the position vector of a wolf.

The coefficient vectors $\vec{A}$ and $\vec{C}$ can be calculated as follows:

$$\vec{A} = 2\vec{a}.\vec{r_1} - \vec{a} \quad (26)$$

$$\vec{C} = 2.\vec{r_2} \quad (27)$$

where $\vec{a}$ is an element that linearly decreased from 2 to 0 over the whole iterations; $\vec{r_1}$ and $\vec{r_2}$ indicate random vectors in [0,1]. To obtain the optimal solution of an optimization problem, the simulated social leadership and encircling mechanism are used in GWO. In this algorithm, the best, second best, and third best are saved, and other search agents are obliged (ω) for updating their positions with respect to them. For each search agent, to mimic the hunting and find favourable regions of the search space, the following mathematical formulations are run constantly during optimization:

$$\overrightarrow{D_\alpha} = |\overrightarrow{C_1}.\vec{X}_\alpha - \overrightarrow{X}| \quad (28)$$

$$\overrightarrow{D_\beta} = |\overrightarrow{C_2}.\vec{X}_\beta - \overrightarrow{X}| \quad (29)$$

$$\overrightarrow{D_\delta} = |\overrightarrow{C_3}.\vec{X}_\delta - \overrightarrow{X}| \quad (30)$$

$$\overrightarrow{X_1} = \overrightarrow{X_\alpha} - \overrightarrow{A_1}.\overrightarrow{D_\alpha} \quad (31)$$

$$\overrightarrow{X_2} = \overrightarrow{X_\beta} - \overrightarrow{A_2}.\overrightarrow{D_\beta} \quad (32)$$

$$\overrightarrow{X_3} = \overrightarrow{X_\delta} - \overrightarrow{A_3}.\overrightarrow{D_\delta} \quad (33)$$

$$\vec{X}(t+1) = \frac{\left(\overrightarrow{X_1} + \overrightarrow{X_2} + \overrightarrow{X_3}\right)}{3} \quad (34)$$

The GWO algorithm's optimization starts by creating a set of random solutions as the first population. The three best solutions which are obtained during the optimization should be saved as α, β, and δ solutions. The other search agents (ω wolves) are updating their positions according to Equations (28)–(34). In the meantime, a and A parameters are decreased in a linear manner over the iteration. Hence, the search agents diverge from the victim when $|\overrightarrow{A}|$ is greater than one while they tend to converge towards the victim $|\overrightarrow{A}|$ is less than one. In the end, the score and position of α solution are returned as the best solutions obtained throughout optimization when an end condition is satisfied.

To perform multi-objective optimization based on GWO, the Multi-Objective Grey Wolf Optimizer (MOGWO) algorithm was proposed and utilized in [40]. The process is like its single objective, as mentioned above. Nevertheless, to employ this algorithm for solving a multi-objective optimization problem, the concept of dominance is utilized. A Pareto archive is responsible for storing and updating a set of non-dominated Pareto

optimal solutions obtained so far. A leader selection strategy is used as the second component to assist in choosing α, β, and δ solutions as the archive's hunting process leaders. The archive is normally set to have a limited size due to computer memory usage. In MOGWO, the adaptive grid (or hypercube segments) algorithm is used to deal with this task. This algorithm should work in which the generated adaptive grids can cover all the current non-dominated solutions. In the most crowded hypercube, the members would be selected randomly and removed from the archive until the number of residual members is equal to the maximum archive size. For choosing α, β, and δ, a roulette wheel is applied in MOGWO to select a segment in which its probability is inversely proportional to its number of members. Three members in the selected segment will be assigned as the leaders. Suppose the segment contains members less than the three leaders. In that case, the roulette wheel selection will be executed for selecting another segment, and the process is repeated until having the three leaders. The MOGWO starting with the initial population and Pareto archive. Then, the roulette wheel and adaptive grid operators are used to select the three leaders. After that, all the search area agents are updated based on Equations (28)–(34). The non-dominated solutions sorted from the combination of members in the previous archive and the new agents' positions are used to update the Pareto archive. The three leaders α, β, and δ are then updated, and the next generation is generated. This process is repeated until a termination criterion is met. It is important to mention that this work's focus is to build a planning model for inverter-based RES not to improve the MOGWO. Consequently, any other optimization technique can be used for solving this RES planning model. The MOGWO has been employed due to its superior performance in wide applications to get global solutions [40].

3.2 | Non-Dominated sort technique

The non-dominated sort technique can be employed to generate the Pareto optimal ranking, which split the obtained solutions into various fronts with different ranks. Therefore, the Pareto optimal technique is employed to trade-off the objective functions and introduce multiple solutions for the optimization problem. The ranking of the solutions is achieved based on the non-dominated sort. The Pareto optimal ranking can be illustrated as given in Figure 1. If x_1 and x_2 are two solutions for a multi-objective optimization problem. Therefore, any of these two solutions can be dominant or non-dominant in the other solution. In the case of a minimization problem, the solution x_1 dominates the solution x_2 if [41]:

$$\forall i \in \{1, 2, \ldots, N_{obj}\} : f_i(x_1) \leq f_i(x_2) \tag{35}$$

$$\forall j \in \{1, 2, \ldots, N_{obj}\} : f_j(x_1) \leq f_j(x_2) \tag{36}$$

where N_{obj} is the number of objective functions, the solution x_1 will not dominate the solution x_2, if any of the above conditions is violated. In the case of dominating of the solution x_1 the solution x_2, the solution x_1 is called the non-dominated solution.

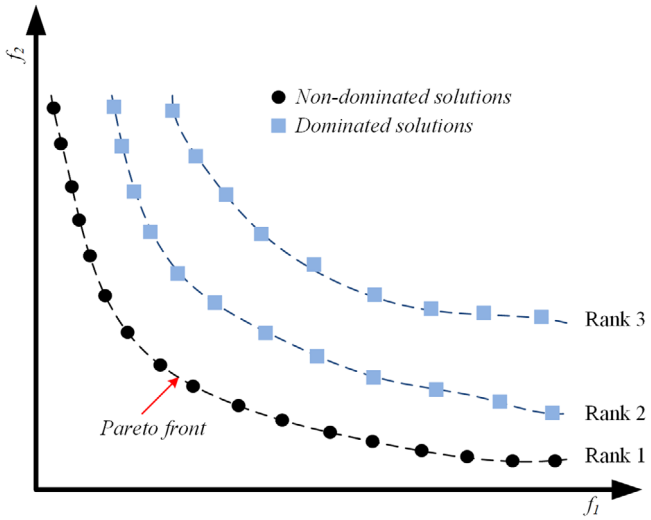

FIGURE 1 Mechanism of non-dominated sorting

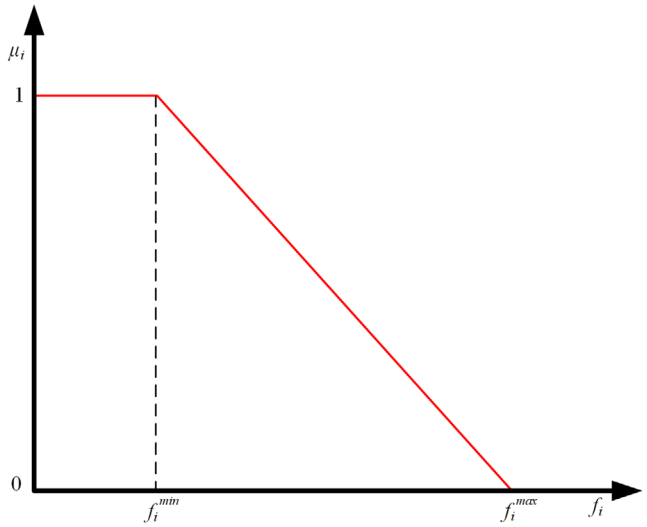

FIGURE 2 The linear membership function

3.3 | Best compromise solution

At the end of MOGWO, the Pareto optimal solution is obtained; it is necessary to choose a solution among the non-dominated solutions. This solution represents the best compromise solution based on the decision maker's requirements. However, the judgment of the decision-maker has inaccurate nature. Hence, it is assumed that the decision-maker has fuzzy nature goals of each objective function. Therefore, the fuzzy set theory is utilized as a decision-maker [42]. The membership functions of the fuzzy set theory represent the targets of each objective function. Based on the experiences and conjectural knowledge of the decision-maker, the membership function can be defined. Here, a simple linear membership function depicted in Figure 2 is considered for each objective function. The

membership function can be described by [41, 43]:

$$\mu_i = \begin{cases} 1, & f_i \le f_i^{min} \\ \dfrac{f_i^{max} - f_i}{f_i^{max} - f_i^{min}}, & f_i^{min} < f_i < f_i^{max} \\ 0, & f_i \ge f_i^{max} \end{cases} \quad (37)$$

where $f_i^{max}$and f_i^{min} represent the maximum and minimum values of ith objective function, respectively. The membership function μ_i varies from 0 to 1, where $\mu_i = 0$ and $\mu_i = 1$ indicate, respectively, the incompatibility and full compatibility of the solution with the set.

For each non-dominated solution k, the normalized membership function μ^k can be determined as follows:

$$\mu^k = \sum_{i=1}^{N_{obj}} \mu_i^k \Big/ \sum_{k=1}^{N_{nd}} \sum_{i=1}^{N_{obj}} \mu_i^k \quad (38)$$

where N_{nd} represents the number of non-dominated solutions. The membership function $\mu^k$is the membership function of non-dominated solutions in a fuzzy set. The solution that has maximum μ^k membership in the fuzzy set is the best compromise solution.

4 | SOLUTION PROCESS

The proposed methodology for optimal planning of inverter-based RES in the microgrids accommodating charging stations of EVs is described in Figure 3. This figure shows that the process has three main phases. In the first phase, reading and preparing the input data, the microgrid data, and the historical dataset of the solar irradiance, wind speed, and load demand have been read. These data are employed to estimate the probabilistic models of the RES and load demand. Furthermore, this phase defines the zones in the microgrid, constraints of the microgrid (e.g. RES constraints, EVs constraints, diesel constraints, and constraints of the inverters), and the EV charging stations' location and charging schemes of the EVs.

In the second phase, developed bi-level optimization, an optimization model is established to solve the planning problem. This model consists of two levels called outer level (main problem) and inner level (sub-problem). MOGWO is employed in the two levels to solve the main and sub-problems of the model. The outer level suggests optimal sizes and locations of the RES and passes them to the inner level. Based on these locations and sizes of the RES, the inner level analysis of the microgrid for 24-h using a power flow solver along with the optimizer to determine the optimal charging/discharging power of the EVs, optimal power of the diesel, and optimal reactive power of the interfacing inverters of the RES. Therefore, the inner level calculates the objective functions (tie-line power and VD) for each state according to their occurrence probability. The total sum of each objective function is utilized as an objective function for the outer level. This indicates that the outer level includes the inner level. Hence, for each iteration of the outer level, the inner level should be completely executed until its convergence.

In the end, the optimal sizes and locations of the RES, optimal charging/discharging power of the EVs, optimal reactive power of the RES inverters, and optimal power of the diesel generator are shown in the third phase. It is important to note that the capital costs and maintenance expenses of RES are not considered in the planning model. Differently, we show the benefits of EVs charging and reactive power capabilities of the interfacing RES inverters.

5 | RESULTS AND DISCUSSIONS

5.1 | Microgrid and dataset

The IEEE 69-bus distribution system is chosen as a microgrid to examine the proposed methodology. The complete line and bus data of the distribution system are obtained from [44, 45]. However, the proposed model in Section 2 is generally formulated to be applied for any other distribution test systems. In this work, this microgrid is split into six different zones (Zone 1, Zone 2,…, Zone 6) as shown in Figure 4. The PV units can be allocated in Zone 1, Zone 2, and Zone 3 while the WT can be allocated in Zone 4, Zone 5, and Zone 6. The microgrid accommodates four charging stations connected to buses 33, 36, 52, and 65 as depicted in Figure 4. The maximum capacity of each charging station is sixty EVs. The arriving times of these EVs during a day follow Figure 5, while the initial SOC for each EV at that time is depicted in Figure 6.

Tesla Model S batteries are used for EVs. The capacity of the utilized battery is 85 kWh [46]. According to the daily nature of the EV' owners, the EVs normally leave the charging station in the morning and back home after working hours. Therefore, it is expected that each EV can connect to the microgrid for 12 h (i.e. 7:00 AM-06:00 PM). Vehicle-to-grid (V2G) technology can be employed during the connecting of the EVs to the microgrid with guaranteeing enough SOC for daily trips at the departure time of each EV. The maximum charging and discharging rate of each EV is 20% of the battery capacity (0.2×85) [47]. Two different types of RES are optimally planned in the microgrid for minimizing the total voltage deviation and the tie-line power between the microgrid and the utility.

Three-years historical datasets of solar irradiance, wind speed, and load demand are used for calculating their probability distribution functions. Here, a day within the three years is used to represent by these years in which it is divided into the 24-h time period. Considering that each year has 365 days, hence, each time period has 1095 data points for solar irradiance, wind speed, and load demand (3 years × 365 days per year). By utilizing these data, at each time period, the mean and standard deviation can be determined, and so the Beta, Weibull, and Normal probability density functions can be generated for each time period. The historical data of solar irradiance, wind speed, and load demand are taken from [48, 49], and [50], respectively. Two different situations are followed for the planning of the

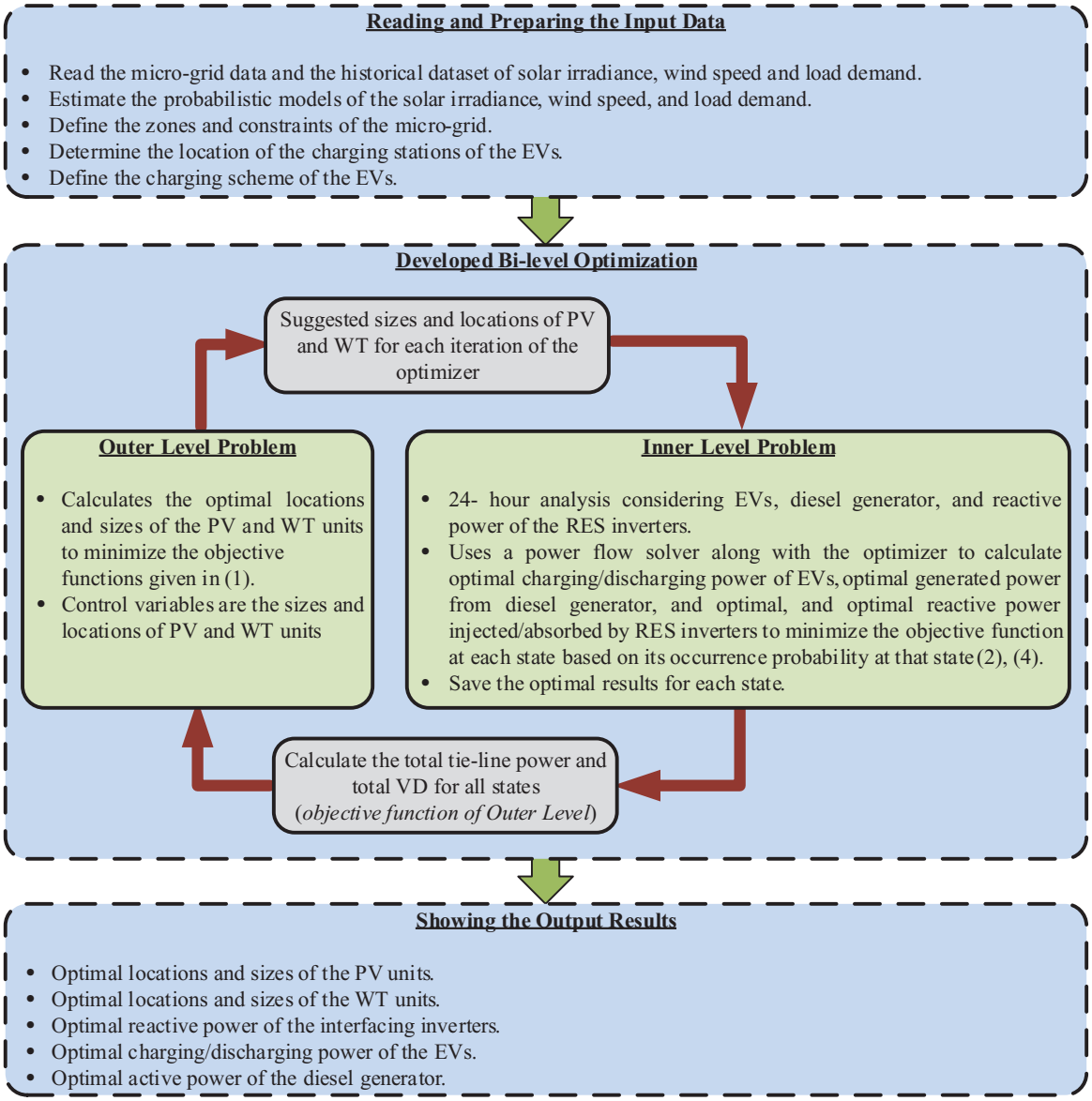

FIGURE 3 Solution process of the proposed methodology

microgrid. In the first situation, the RES (PV and WT) are optimally planned the microgrids with applicability for transferring an amount of the power between the microgrid and the utility. In contrast, the second situation the planning of the RES is done considering autonomous microgrid in which the tie-line power between the microgrid and the utility is zero. The proposed methodology is performed in the cases of disabling and enabling the reactive power capability of the interfacing inverters of the RES. We have written the code of the optimization problem (MOGWO optimization algorithm and the planning model of the inverter-based RES) in MATLAB 2017b, and this program has been carried out on a Core I5 PC with 8GB RAM. The maximum iterations and populations of the optimizer for both levels are 100 and 50, respectively.

5.2 | Case studies

To evaluate the efficiency of the proposed methodology for optimal planning of the inverter-based RES, four different cases have been carried out and compared to allocate a mix of three PV units and three WT units in the grid-connected microgrid which accommodates EV charging stations. The different four cases can be explained as follows:

- Case 1: In this case, the RES are optimally planned in the microgrid without considering neither reactive power support from the RES inverters nor EVs.
- Case 2: This case considers only the EV charging/discharging.

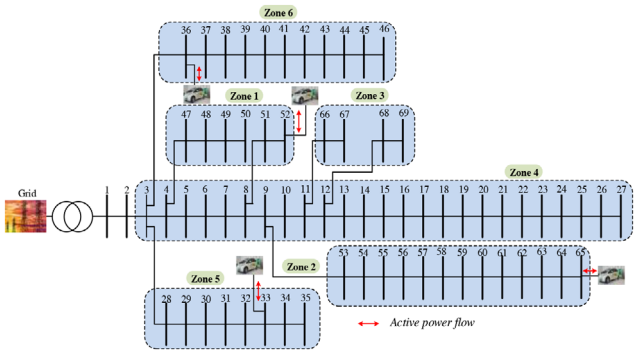

FIGURE 4 Single-line diagram of the IEEE 69-bus distribution system

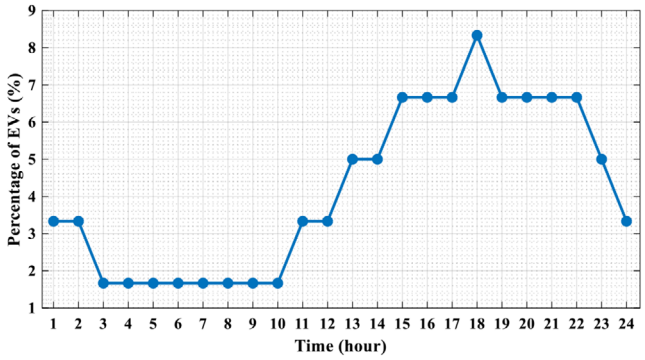

FIGURE 5 Distribution of the EVs at the charging stations throughout a day

- Case 3: In this case, the EV charging/discharging, and the reactive power support of the RES inverters are considered.
- *Case 4*: This case is like the previous case (Case 3) while a diesel generator at bus 6 is considered here.

In this work, we have carried out ten runs for each simulated case study while the best solution among them is chosen as the final solution. Further, it is assumed that all EVs are equipped with Tesla Model S, while the proposed model can adopt any other battery models.

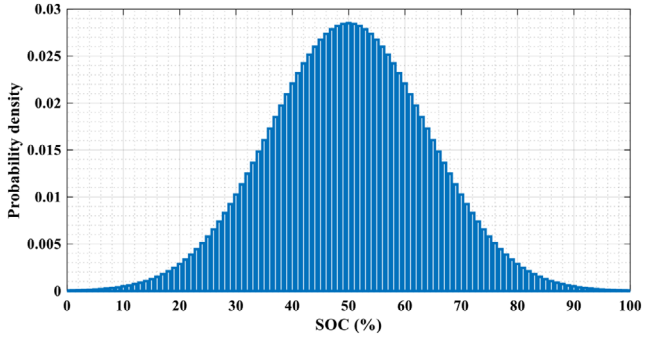

FIGURE 6 Probability distribution function of EV initial SOC

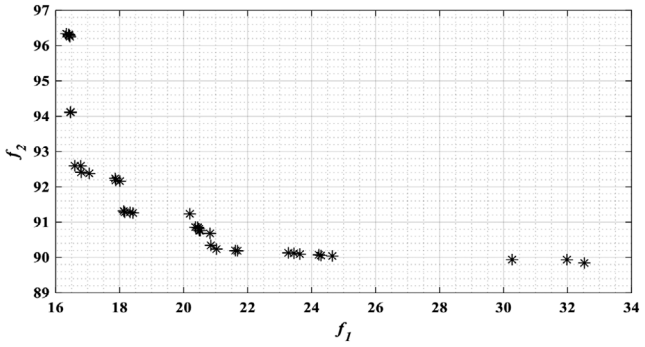

FIGURE 7 Pareto-optimal solutions obtained for combined in Case 1

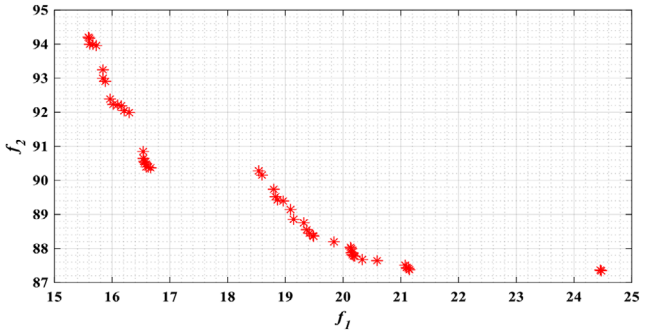

FIGURE 8 Pareto-optimal solutions obtained for combined in Case 2

5.3 | Analysis of the cases

In Cases 1 and 2, the inverters of the RES are working at unity power factor while in Cases 3 and 4, the RES inverters have the DSTATCOM functionality in which they can inject/absorb the reactive power to/from the microgrid based on the amount of generated active power by the RES. Furthermore, the effect of EVs charging/discharging on the planning problem is considered in Cases 2, 3, and 4 while the EVs are considered to charge with a fixed rate of 20% of the total capacity regardless of the system state is considered in Case 1.

The set of dominant points (f_1 and f_2) for the four different cases are depicted in Figures 7–10. The optimal sites and sizes of the PV units and WT units which are computed by employing the different cases along with the values of the corresponding

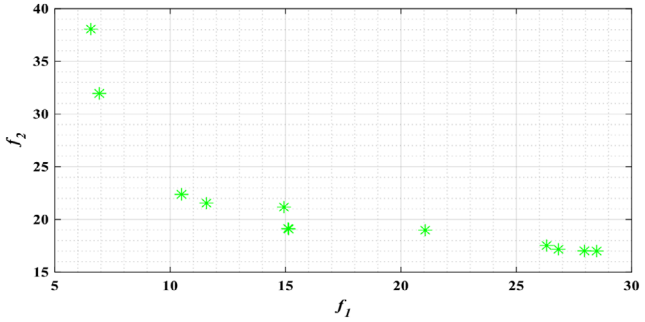

FIGURE 9 Pareto-optimal solutions obtained for combined in Case 3

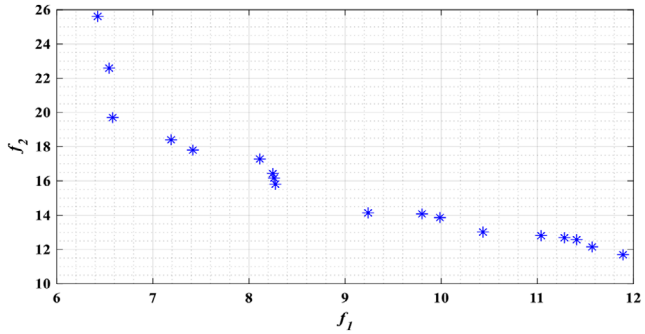

FIGURE 10 Pareto-optimal solutions obtained for combined in Case 4

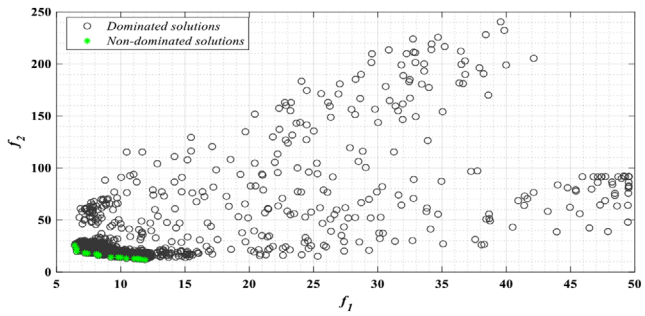

FIGURE 11 Pareto-optimal solutions obtained in case 4 including all solutions (dominated and non-dominated solutions)

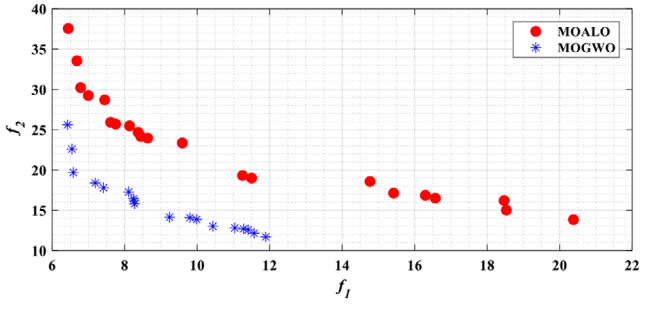

FIGURE 12 Pareto-optimal solutions obtained in case 4 using MOALO and MOGWO

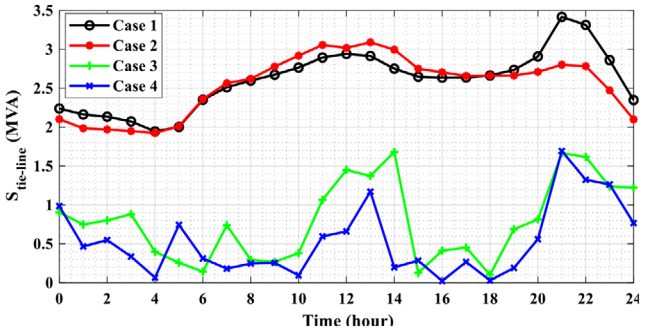

FIGURE 13 Hourly tie-line power between the utility and the microgrid for the four different cases

average voltage deviation and average tie-line power are given in Table 1. Figures 7–10 and Table 1 show that Case 4 gives better results compared to the other cases in terms of voltage magnitude deviation and tie-line power in which they are significantly decreased. For instance, the voltage deviation reductions in Case 2, Case 3, and Case 4 compared to Case 1 are 1.89%, 40%, and 57%, respectively. On the other hand, the values of the tie-line power are decreased by 5%, 73%, and 81% in the case of Case 2, Case 3, and Case 4, respectively, compared to the Case1. It can be noted that the optimal locations and sizes of the RES differ according to the applied case as illustrated in Table 1. Figure 11 shows the Pareto-optimal solutions obtained in Case 4 including all solutions (dominated and non-dominated solutions). Multi-objective ant lion optimizer (MOALO) is employed to solve the proposed approach and compared with MOGWO in Figure 12. This figure shows the superiority of MOGWO over MOALO to get best optimal solutions.

The hourly active tie-line power between the utility and the microgrid and the voltage magnitude deviation are displayed in Figures 13 and 14, respectively. These figures show that enabling the reactive power capability of the RES inverters can significantly reduce the tie-line power and the voltage magnitude deviation as in Case 3 and Case 4. However, the hourly tie-line power and the voltage magnitude deviation in Case 4 are lower than those in the other cases. This is thanks to simultaneous optimization of reactive power of the interfacing inverters, EV charging/ discharging, and the active power of the diesel generator. The optimal reactive powers of the RES inverters

TABLE 1 Computed results for 69-bus distribution system

Item	Case 1			Case 2			Case 3			Case 4		
PV locations	47	61	66	47	63	66	50	62	66	48	61	67
WT locations	14	32	40	12	29	40	20	34	45	23	29	42
PV sizes (MW)	0.67	2.61	0.10	0.78	1.98	0.76	0.10	2.21	0.40	0.20	2.01	0.80
WT sizes (MW)	1.97	1.54	0.58	2.44	1.42	0.75	0.81	0.92	2.24	0.82	1.00	0.27
Average voltage deviation (pu)	0.53			0.52			0.32			0.23		
Voltage deviation reduction (%)	—			1.89			40			57		
Average tie-line power (MVA)	2.61			2.48			0.71			0.50		
Reduction of tie-line power (%)	—			5			73			81		

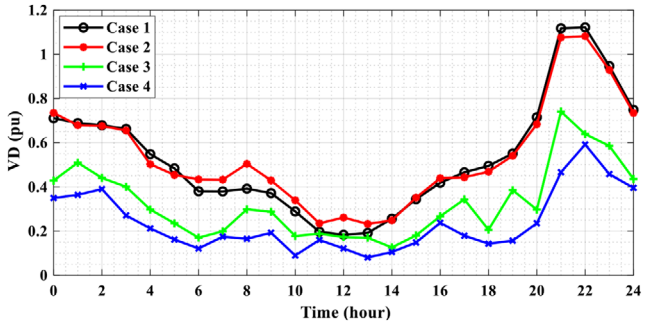

FIGURE 14 Hourly voltage magnitude deviation for the four different cases

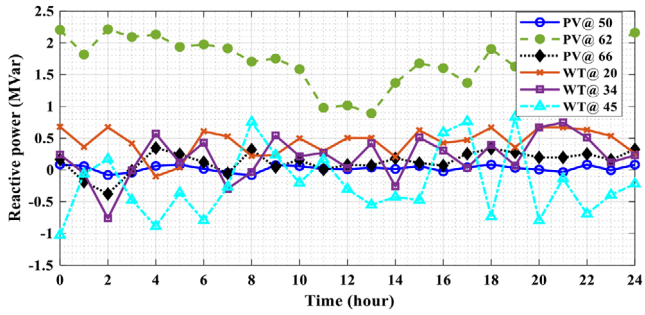

FIGURE 15 Hourly reactive power of the RES inverters for Case 3

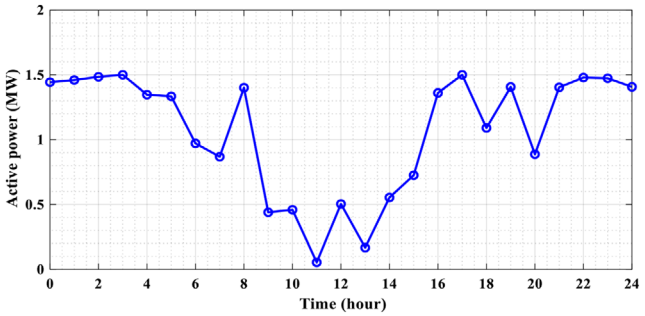

FIGURE 17 Hourly active power of the diesel generator for Case 4

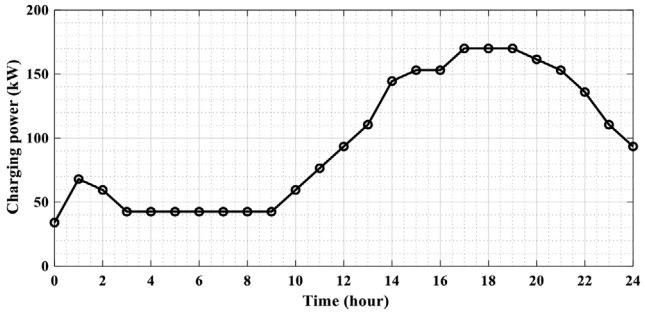

FIGURE 18 Hourly charging power of the EVs at charging station connected to bus 36 for Case 1

injected/absorbed to/from the microgrid for Case 3 and Case 4 are given in Figures 15 and 16, respectively. It is worth mentioning that the positive values mean that the RES inverters inject the reactive powers to the microgrid, while the negative values indicate that the inverters absorb the reactive powers from the microgrid. On the other hand, the optimal hourly active power of the diesel generator which is employed in Case 4 is depicted in Figure 17. The optimized reactive powers of RES inverters and active power of the diesel generator along with the charging/discharging power of the EVs can greatly contribute for minimizing the objective functions.

Regarding the charging/discharging power of the EVs, Figures 18 and 19 show the charging power and SOC of the EVs in Case 1. In this case, EVs are considered to charge once they arrived at the charging station with a fixed rate of 20% of the total capacity regardless of the system. To avoid the repetition of the result, only the charging/discharging powers and SOC of the EVs connected to the charging station at bus 36 are depicted here. It is important to mention that, in this work, the EVs that arrive at the end of the previous day have been considered, in which they have to continue charging at the beginning of the next day. Figure 19 shows that the SOC of all EVs at departure time is 100%. The charging and discharging powers for Cases 2, 3, and 4, in which the V2G technology is employed, are shown in Figure 20. The positive values indicate that the EVs are charging from the microgrid while the negative powers indicate that they are discharging to the microgrid. Figure 21 illustrates the SOC of the EVs at the charging station connected to bus 36 for Case 4. The SOC in Cases 2 and 3 follow the same trend. Therefore, they have not been shown here. It is clear that the EVs can charge and discharge to the microgrid (i.e. the SOC are

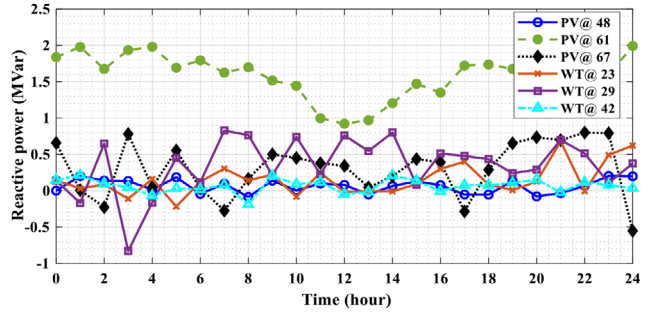

FIGURE 16 Hourly reactive power of the RES inverters for Case 4

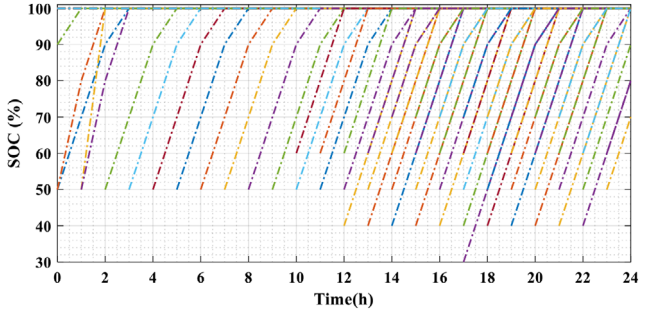

FIGURE 19 SOC of the EVs connected to bus 36 for Case 1

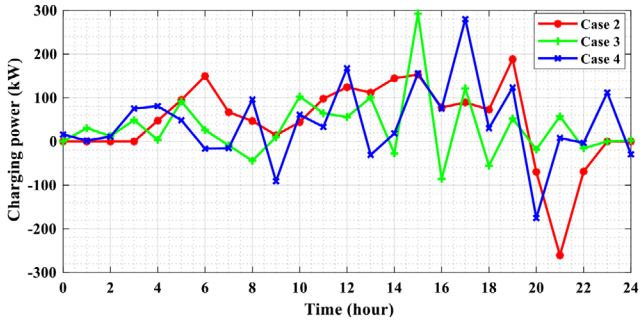

FIGURE 20 Hourly charging/discharging powers of the EVs at charging station connected to bus 36 for Cases 2, 3, and 4

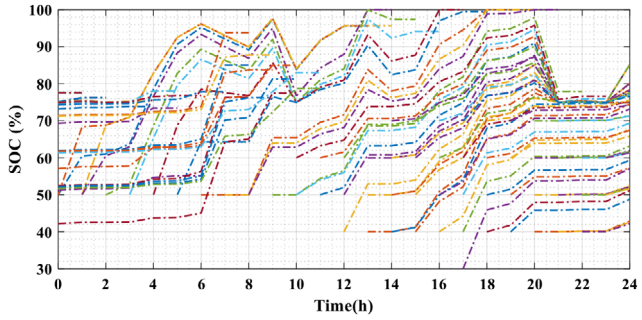

FIGURE 21 SOC of the EVs connected to bus 36 for Case 4

increasing and decreasing) while the SOC of all EVs at parting time is high enough for daily trips.

5.4 | Application to autonomous microgrid

In this subsection, the proposed methodology is applied for the autonomous operation of the microgrid. For this purpose, Case 4 is applied here with giving the full priority to the objective function of the tie-line power between the microgrid and the utility. The optimal locations, optimal sizes, average voltage magnitude deviation, and average tie-line power by employing this case are given in Table 2. This table shows that the average tie-line power is zero. This indicates that the microgrid is autonomous in which the load demand in the microgrid is fed only by the RES and diesel generator. It is important to note that the optimal locations and sizes of PV units and WT units are changed compared to Case 4 in the case of the grid-connected microgrid. For instance, the optimal locations of the PV units are buses 50, 54, and 66, while the optimal locations of the WT units are buses 26, 28, and 44. On the other hand, the optimal sizes of the PV units are 0.36, 0.54, and 0.16 MW, respectively. The optimal sizes of the WT units are 0.85, 0.11, and 3.55 MW, respectively. The hourly voltage magnitude deviation and tie-line power are shown in Figure 22, while the active power of the diesel generator is depicted in Figure 23. Moreover, the optimal reactive powers of the interfacing inverters are displayed in Figure 24.

TABLE 2 Obtained results in the case of autonomous operation of the microgrid

Item	Case 5		
PV locations	50	54	66
WT locations	26	28	44
PV sizes (MW)	0.36	0.54	0.16
WT sizes (MW)	0.85	0.11	3.55
Average voltage deviation (pu)	1.26		
Average tie-line power (MVA)	0.0		

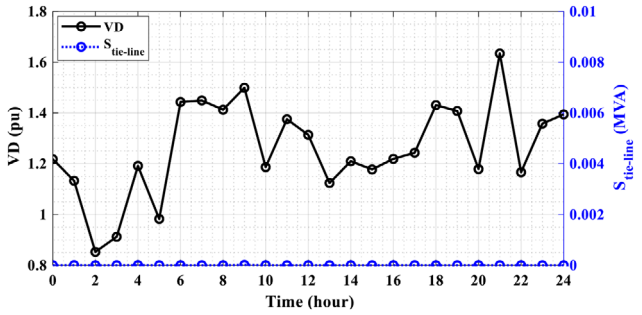

FIGURE 22 Hourly voltage magnitude deviation and tie-line power in the case of autonomous microgrid

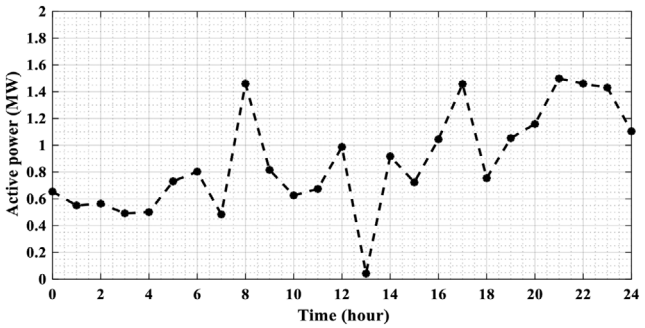

FIGURE 23 Hourly active power of the diesel generator in the case of autonomous microgrid

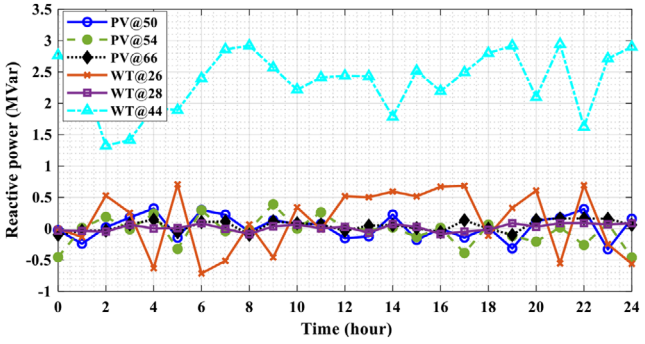

FIGURE 24 Hourly reactive power of the RES inverters in the case of autonomous microgrid

6 | CONCLUSIONS

The optimal planning of microgrids is challenging with the uncertain generation of PV and WT systems and stochastic EV models. To address these issues, the best locations and sizes of photovoltaic and wind energy units in microgrids with EV charging stations are accurately calculated in this study using an optimization methodology to achieve autonomous microgrids. In particular, this introduced method considers generation profile intermittency in PV and wind energy systems, total load requirement, DSTATCOM operational capacity of inverter-based photovoltaic and wind generation stations, and microgrid branch and node restrictions. EV requirements are also taken into account, including initial and predetermined SOC schedules, arrival and departure hours, and various regulated and unregulated charging techniques. Accordingly, we have developed a bi-level metaheuristic-based optimization approach to efficiently deliver accurate solutions for this multipart planning model. The outer level (main problem) and inner level (sub-problem) functions are used to maximize renewable energy sources and EV decision variables, respectively. Total voltage deviations and grid energy are considered sub-objectives that must be optimized. The feasibility of the potential solution is determined by a sequence of experiments and case studies. The voltage deviation and the tie-line power reductions by the proposed method are 57% and 81%, respectively, which is higher than those of the existing approaches. The findings indicate that the suggested method for designing renewable energy sources and monitoring EVs is successful in achieving autonomous microgrids with EV charging stations interconnected to photovoltaic and wind generation units. In this work, we have not considered the microgrid islanding mode, and will be considered in a future study.

Nomenclature

$\vec{X}_p$ position vector of the victim
$\vec{r}_1, \vec{r}_2$ random vectors in [0,1]
$\vec{A}, \vec{C}$ coefficient vectors
$C_{PV,i}$ capacity of PV unit
$C_{PV,i}^{max}$ highest capacity of PV unit at bus i
$C_{PV,i}^{min}$ lowest capacity of PV unit at bus i
$C_{WT,i}$ capacity of WT unit
$C_{WT,i}^{max}$ highest capacity of WT unit at bus i
$C_{WT,i}^{min}$ lowest capacity of WT unit at bus i
$I_{ij,s}^{t}$ the current flows in line ij
I_{ij}^{max} maximum allowed current rate
N_{WTi}^{max} maximum allowed number of WT units at bus i
N_{WTi}^{min} minimum allowed number of WT units at bus i
$P_{C,j,s}^{t}$ charging station power at bus j for state s
$P_{D,i,s}^{t}$ load demand at bus i for state s during segment t
$P_{Diesel,i,s}^{t}$ active power output of the diesel generator
$PM^{t}(\lambda_s)$ amalgamated probability model of the solar irradiance, wind speed, and demand load
$P_{PV,i,s}^{t}$ power output of PV unit
$P_{TL,s}^{t}$ the amount of tie-line power fed by the main grid
$P_{WT,i,s}^{t}$ power output of WT unit
$P_{c,i,s}^{max,t}$ maximum charging station power
$P_{c,i,s}^{min,t}$ minimum charging station power
$Q_{D,i,s}^{t}$ reactive power demand at bus i for state s
$Q_{Diesel,i,s}^{max,t}$ highest reactive power of diesel generator at bus i
$Q_{Diesel,i,s}^{min,t}$ lowest reactive power of diesel generator at bus i
$Q_{I,PV,i,s}^{max}$ highest reactive power of PV at bus i
$Q_{I,PV,i,s}^{min}$ lowest reactive power of PV at bus i
$Q_{I,PV,i,s}^{t}$ reactive power of the PV interfacing inverter
$Q_{I,WT,i,s}^{max}$ highest reactive power of WT at bus i
$Q_{I,WT,i,s}^{min}$ lowest reactive power of WT at bus i
$Q_{I,WT,i,s}^{t}$ reactive power of the WT interfacing inverter
R_{PV}^{max} maximum total PV power
R_{PV}^{max} maximum total WT power
VD_s^t total voltage deviations of distribution system for the state s during time segment t
$\vec{X}$ position vector of a wolf
$\vec{a}$ an element that linearly decreased from 2 to 0 over the whole iterations
f_i^{max}, f_i^{min} maximum and minimum values of i^{th} objective function
$prob_R^t(G_x)$ solar irradiance probability of state x
$prob_l^t(G_z)$ load demand probability of state z
$prob_w^t(G_y)$ wind speed probability of state y
$\delta_{ij,s}^{t}$ voltage angles variance at i^{th} and j^{th} nodes
μ_i membership function
ϕ_b set of the system buses
B_{ij} susceptance of line ij
G_{ij} conductance of line ij
N_B number of nodes
N_{nd} number of non-dominated solutions
N_{obj} number of objective functions
n_s number of the states
n_t number of time segments
N_{WTi} number of WT units at bus i
$S_{I,PV,i}$ inverter rating of PV
$S_{I,WT,i}$ inverter rating of WT
$SOC_{n,d,s}$ SOC of n^{th} battery at departure time
$SOC_{n,min}$ minimum SOC set by the vehicle's owner
V_i voltage magnitude at bus i
V^{max} highest voltage limit
V^{min} lowest voltage limit
V_n normal voltage magnitude
x_1 non-dominated solution
x_2 dominated solution
α the best solution
β second best solution
δ third best solution
λ a matrix with two columns which comprises all possible amalgamations of PV power, WT power and the load demand states
ψ complete probability model

REFERENCES

1. Al-Shetwi, A.Q., et al.: Grid-connected renewable energy sources: Review of the recent integration requirements and control methods. J. Cleaner Prod. 253, 119831 (2020)
2. Kumar, S., et al.: Reliability enhancement of electrical power system including impacts of renewable energy sources: A comprehensive review. IET Gener. Transm. Distrib. 14(10), 1799–1815 (2020)
3. Morstyn, T., Hredzak, B., Agelidis, V.G.: Control strategies for microgrids with distributed energy storage systems: An overview. IEEE Trans. Smart Grid 9(4), 3652–3666 (2018)
4. Ali, A., Mahmoud, K., Lehtonen, M.: Multi-objective photovoltaic sizing with diverse inverter control schemes in distribution systems hosting EVs. IEEE Trans. Ind. Inf. 17(9), 5982–5992 (2020)
5. Sun, X., Qiu, J.: Two-stage Volt/Var control in active distribution networks with multi-agent deep reinforcement learning method. IEEE Trans. Smart Grid. 12, 2903-2912 (2021)
6. Mahmoud, K., Lehtonen, M.: Comprehensive analytical expressions for assessing and maximizing technical benefits of photovoltaics to distribution systems. IEEE Trans. Smart Grid (2021). doi:10.1109/TSG.2021.3097508
7. Ali, A., Raisz, D., Mahmoud, K.: Voltage fluctuation smoothing in distribution systems with RES considering degradation and charging plan of EV batteries. Electr. Power Syst. Res. 176, 105933 (2019)
8. Ali, A., Raisz, D., Mahmoud, K.: Optimal scheduling of electric vehicles considering uncertain RES generation using interval optimization. Electr. Eng. 100(3), 1675–1687 (2017)
9. Qiu, D., et al.: A deep reinforcement learning method for pricing electric vehicles with discrete charging levels. IEEE Trans. Ind. Appl. 56(5), 5901–5912 (2020)
10. Xie, R., et al.: Optimal service pricing and charging scheduling of an electric vehicle sharing system. IEEE Trans. Veh. Technol. 69(1), 78–89 (2020)
11. Fathabad, A.M., et al.: Data-driven planning for renewable distributed generation integration. IEEE Trans. Power Syst. 35(6), 4357–4368 (2020)
12. Atwa, Y.M., et al.: Optimal renewable resources mix for distribution system energy loss minimization. IEEE Trans. Power Syst. 25(1), 360–370 (2010)
13. Mahmoud, K., Abdel-Nasser, M.: Fast yet accurate energy-loss-assessment approach for analyzing/sizing PV in distribution systems using machine learning. IEEE Trans. Sustainable Energy 10(3), 1025–1033 (2019)
14. Mahmoud, K., Yorino, N., Ahmed, A.: Optimal distributed generation allocation in distribution systems for loss minimization. IEEE Trans. Power Syst. 31(2), 960–969 (2016)
15. Vatani, M., et al.: Multiple distributed generation units allocation in distribution network for loss reduction based on a combination of analytical and genetic algorithm methods. IET Gener. Transm. Distrib. 10(1), 66–72 (2016)
16. Vahidinasab, V.: Optimal distributed energy resources planning in a competitive electricity market: Multiobjective optimization and probabilistic design. Renewable Energy 66, 354–363 (2014)
17. Farh, H.M.H., et al.: A novel crow search algorithm auto-drive pso for optimal allocation and sizing of renewable distributed generation. IEEE Access 8, 27807–27820 (2020)
18. Ali, A., et al.: Optimal placement and sizing of uncertain PVs considering stochastic nature of PEVs. IEEE Trans. Sustainable Energy 11(3), 1647–1656 (2020)
19. Ali, A., Mahmoud, K., Lehtonen, M.: Enhancing hosting capacity of intermittent wind turbine systems using bi-level optimisation considering OLTC and electric vehicle charging stations. IET Renewable Power Gener. 14(17), 3558–3567 (2020)
20. Pereira, B.R., et al.: Optimal distributed generation and reactive power allocation in electrical distribution systems. IEEE Trans. Sustainable Energy 7(3), 975–984 (2016)
21. Ganguly, S., Samajpati, D.: Distributed generation allocation on radial distribution networks under uncertainties of load and generation using genetic algorithm. IEEE Trans. Sustainable Energy 6(3), 688–697 (2015)
22. Eid, A., et al.: An enhanced artificial ecosystem-based optimization for optimal allocation of multiple distributed generations. IEEE Access 8, 178493–178513 (2020)
23. Ramadan, A., et al.: Scenario-based stochastic framework for optimal planning of distribution systems including renewable-based dg units. Sustainability 13(6), 3566 (2021)
24. Mitra, J., Vallem, M.R., Singh, C.: Optimal deployment of distributed generation using a reliability criterion. IEEE Trans. Ind. Appl. 52(3), 1989–1997 (2016)
25. Bagheri Tolabi, H., Ali, M.H., Rizwan, M.: Simultaneous reconfiguration, optimal placement of DSTATCOM, and photovoltaic array in a distribution system based on fuzzy-ACO approach. IEEE Trans. Sustainability Energy 6(1), 210–218 (2015)
26. Aghamohamadi, M., Mahmoudi, A., Haque, M.H.H.: Adaptive robust recourse-based bidding strategy and capacity allocation of PV-WT-BES owning prosumers under uncertainties. IEEE Trans. Ind. Appl. 57(4), 4170–4186 (2021)
27. Jeon, S.U., et al.: Practical power management of PV/ESS integrated system. IEEE Access 8, 189775–189785 (2020)
28. Amer, A., et al.: Stochastic planning for optimal allocation of fast charging ctations and wind-based DGs. IEEE Syst. J. 1-11, (2020). doi:10.1109/JSYST.2020.3012939
29. Mehrjerdi, H.: Dynamic and multi-stage capacity expansion planning in microgrid integrated with electric vehicle charging station. J. Energy Storage 29, 101351 (2020)
30. Clairand, J.M., et al.: Power generation planning of galapagos. microgrid considering electric vehicles and induction stoves. IEEE Trans. Sustainable Energy 10(4), 1916–1926 (2019)
31. Aluisio, B., et al.: Planning and reliability of DC microgrid configurations for electric vehicle supply infrastructure. Int. J. Electr. Power Energy Syst. 131, 107104 (2021)
32. Clairand, J.M., et al.: Impact of electric vehicle charging strategy on the long-term planning of an isolated microgrid. Energies 13(13), 3455 (2020)
33. Yoon, S.G., Kang, S.G.: Economic microgrid planning algorithm with electric vehicle charging demands. Energies 10(10), 1487 (2017)
34. Alharbi, T., Bhattacharya, K., Kazerani, M.: Planning and operation of isolated microgrids based on repurposed electric vehicle batteries. IEEE Trans. Ind. Inf. 15(7), 4319–4331 (2019)
35. Salama, H.S., et al.: Studying impacts of electric vehicle functionalities in wind energy-powered utility grids with energy storage device. IEEE Access 9, 45754–45769 (2021)
36. Ali, A., et al.: Probabilistic approach for hosting high PV penetration in distribution systems via optimal oversized inverter with Watt-Var functions. IEEE Syst. J. 15(1), 684–693 (2021)
37. Ali, A., et al.: Optimal allocation of inverter-based WTGS complying with their DSTATCOM functionality and PEV requirements. IEEE Trans. Veh. Technol. 69(5), 4763–4772 (2020)
38. Ali, A., Mahmoud, K., Lehtonen, M.: Maximizing hosting capacity of uncertain photovoltaics by coordinated management of OLTC, VAr sources and stochastic EVs. Int. J. Electr. Power Energy Syst. 127, 106627 (2021)
39. Mirjalili, S., Mirjalili, S.M., Lewis, A.: Grey wolf optimizer. Adv. Eng. Software 69, 46–61 (2014)
40. Mirjalili, S., et al.: Multi-objective grey wolf optimizer: A novel algorithm for multi-criterion optimization. Expert Syst. Appl. 47, 106–119 (2016)
41. Ghasemi, A., Valipour, K., Tohidi, A.: Multi objective optimal reactive power dispatch using a new multi objective strategy. Int. J. Electr. Power Energy Syst. 57, 318–334 (2014)
42. Roy Ghatak, S., Sannigrahi, S., Acharjee, P.: Multi-objective approach for strategic incorporation of solar energy source, battery storage system, and DSTATCOM in a smart grid environment. IEEE Syst. J. 2, 1–12 (2018)
43. Wu, L.H., et al.: Environmental/economic power dispatch problem using multi-objective differential evolution algorithm. Electr. Power Syst. Res. 80(9), 1171–1181 (2010)
44. Baran, M.E., Wu, F.F.: Network reconfiguration in distribution systems for loss reduction and load balancing. IEEE Trans. Power Delivery 4(2), 1401–1407 (1989)

45. Ali, A., Raisz, D., Mahmoud, K.: Optimal oversizing of utility-owned renewable DG inverter for voltage rise prevention in MV distribution systems. Int. J. Electr. Power Energy Syst. 105, 500–513 (2019)
46. Wu, X., et al.: Stochastic control of smart home energy management with plug-in electric vehicle battery energy storage and photovoltaic array. J. Power Sources 333, 203–212 (2016)
47. Shafiee, S., Fotuhi-Firuzabad, M., Rastegar, M.: Investigating the impacts of plug-in hybrid electric vehicles on power distribution systems. IEEE Trans. Smart Grid 4(3), 1351–1360 (2013)
48. Andreas, A. & Stoffel, T.: Nevada Power: Clark Station; Las Vegas, Nevada (Data). NREL Report No. DA-5500-56508. https://midcdmz.nrel.gov/npcs/. Accessed 15 Jan 2021
49. Historical Climate Data - Climate - Environment and Climate Change Canada. http://climate.weather.gc.ca/ (2019). Accessed 20 Aug 2019
50. European Network of Transmission System Operators for Electricity. https://www.entsoe.eu/ (2020). Accessed 01 Jan 2020

How to cite this article: Ali, A., Mahmoud, K., Lehtonen, M.: Optimal planning of inverter-based renewable energy sources towards autonomous microgrids accommodating electric vehicle charging stations. IET Gener. Transm. Distrib. 16, 219–232 (2022). https://doi.org/10.1049/gtd2.12268